International Journal of Emerging Electric Power Systems

Volume 8, *Issue* 5 2007 *Article* 4

Synchronous Generators Modeling and Control Using the Framework of Individual Channel Analysis and Design: Part 1

Carlos Ernesto Ugalde Loo* Luigi Vanfretti†

Eduardo Liceaga-Castro‡ Enrique Acha**

*University of Glasgow, C.Ugalde@elec.gla.ac.uk

†Rensselaer Polytechnic Institute, vanfrl@rpi.edu

‡Universidad Carlos III de Madrid, edcastro@ing.uc3m.es

**University of Glasgow, E.Acha@elec.gla.ac.uk

Synchronous Generators Modeling and Control Using the Framework of Individual Channel Analysis and Design: Part 1

Carlos Ernesto Ugalde Loo, Luigi Vanfretti, Eduardo Liceaga-Castro, and Enrique Acha

Abstract

In this paper a comprehensive dynamical assessment of a high order synchronous generator plant is carried out using the Individual Channel Analysis and Design (ICAD) framework –a multivariable control engineering tool that allows robustness and system performance evaluations. The great benefits of ICAD are elucidated and contrasted to those provided by the long-time honored block diagram representations. Several models used for the small signal stability analysis of synchronous generators are evaluated under the framework of ICAD. The study, which builds on pioneering work, reveals the great advantages of carrying out control system analysis and design with higher order generator models. Moreover, careful analysis of the ICAD's Multivariable Structure Function (MSF) helps to explain, formally, why some operating conditions of the control system are more critical than others. Furthermore, correct interpretations of MSFs are amenable to robust and stable control system designs. Two kinds of studies are considered in the paper; one assesses operation under various power factor conditions and the other under a varying tie-line reactance. The control system design and stability and structural robustness assessment of the system are presented in the second part of this paper. Moreover, results obtained under the ICAD framework are compared with those arising from conventional controllers.

KEYWORDS: synchronous generators, Individual Channel Analysis and Design, robustness, multivariable control systems

Introduction

Owing to the physical insight afforded by the Heffron-Phillips representation of the synchronous generator (initially introduced by Heffron and Phillips, 1952, and then explored further by DeMello and Concordia, 1969, and Saidy and Hughes, 1994), the model has been widely used and applied to One Machine-Infinite Bus (OMIB) systems. Extensions have been made to include Power System Stabilizers (PSS), sub-transient effects of damper windings and electronically controlled compensation (see, for instance, the work of Aree and Acha, 1999). A major asset of the Heffron-Phillips block diagram model is that it lends itself to the use of classical and robust control techniques, as pointed out by Rogers (2000). However, a drawback of the block diagram representation is that the visual simplicity of this approach is lost when applied to cases of even two machines. On the other hand, eigenanalysis remains as the industry's preferred approach for assessing small signal stability owing to its large-scale applicability as discussed by Kundur et al. (1990); although it may be argued that the great physical insight afforded by the Heffron-Phillips model is not apparent in the eigenanalysis-based solutions.

On the quest for an alternative analysis tool which does not suffer from lack of physical transparency but which would still be applicable to large-scale systems, a classical oriented framework introduced by O'Reilly and Leithead (1991) for multivariable systems, termed *Individual Channel Analysis and Design* (ICAD), has been applied to OMIB systems and other contrived power systems dynamic problems, as shown in the work of Fadlalmoula et al. (1998), Edwards et al. (2000), and Dudgeon et al. (2000). The work of Liceaga-Castro et al. (2005b, 2006) presents ICAD as an induction motor control scheme and a flux generator model has been used in the control of an OMIB system by Ugalde-Loo et al. (2005).

ICAD allows analysis and synthesis of multivariable control design by applying techniques based on Bode/Nyquist plots. The design process involves individual input-output channels definition in terms of a Multivariable Structure Function (MSF), an information rich function with which it is possible to assess the robustness and performance of multivariable control design. Throughout this work (Parts 1 and 2) it is shown that an appropriate interpretation of the MSF provides an effective and complete framework (not a method) for the analysis and control system design of the 2x2 synchronous generator problem.

Fundamental studies of OMIB systems using block diagrams and ICAD have shown to be very useful in understanding key aspects of synchronous machine modeling and the impact of power electronics controllers on the generator dynamic performance. Building on this positive experience, and in the quest for a truly multi-machine, multi-controller environment which yields physical insight,

Part 1 of this paper addresses the modeling of higher order generator representation under the ICAD framework. It also carries out additional fundamental work which has so far received no attention, more specifically, the OMIB system analysis with particular reference to reactive power control. Moreover, the adequacy of several generator order models is critically examined. System performance is studied for different operating conditions and variations in the tie-line reactance of the OMIB system. ICAD analysis of the dynamical structure of the system is presented and compared with that obtained using block diagram representations. Key features of the models used are highlighted. ICAD, as the control strategy for OMIB systems, has been reported by Fadlalmoula et al. (1998) and Ugalde-Loo et al. (2005), with preliminary work on the suitability of the various synchronous generator order models available for analysis in the work of Ugalde-Loo et al. (2006), with more conclusive results presented in this paper. Control system design and stability and structural robustness assessment are addressed in the second part of this paper. For completeness, results obtained under the ICAD framework are compared with those arising from conventional controllers. On the whole, Part 1 and Part 2 of this paper provide a complete modeling and control system design study for higher order synchronous generator models.

1. Block Diagram Modeling of Synchronous Generators

The synchronous machine dynamic representation used to derive all models presented in the paper is based on the work of Hammons and Winning (1971). The stator resistance is assumed to be negligible.

1.1. Model 1 *(5th order, two-axes)*

The following equations in the *s*-domain characterize Model 1.

$$\Delta P_e(s) = K_1\Delta\delta(s) + K_2\Delta E_q''(s) - K_{2d}\Delta E_d''(s) \tag{1}$$

$$\Delta E_t(s) = K_5\Delta\delta(s) + K_6\Delta E_q''(s) + K_{6d}\Delta E_d''(s) \tag{2}$$

$$\Delta E_q''(s) = K_3(s)\Delta E_{fd}(s) - K_4(s)\Delta\delta(s) \tag{3}$$

$$\Delta E_d''(s) = K_{4d}(s)\Delta\delta(s) \tag{4}$$

$$\Delta\omega(s) = \frac{1}{2Hs}\left[\Delta P_m(s) - \Delta P_e(s) - D\Delta\omega(s)\right] \tag{5}$$

$$\Delta\delta(s) = \frac{\omega_0}{s}\Delta\omega(s) \tag{6}$$

where the parameters of equations (1)–(4) are given in the Appendix 2.

Equations (1)–(6) are used to form the block diagram representation for this model, which is shown in figure 1. Notice that the controllers for terminal voltage and speed are included in the block diagram.

1.2. Model 2A *(4th order, two-axes)*

Simplifications may be made in Model 1 in an attempt to reduce modeling complexity and computing overheads while still retaining key generator dynamics effects. To this end, the sub-transient effects that produce a demagnetizing effect due to a change in the rotor by the damping winding are neglected in this model. However, the transient effects of the damping windings are still taken into account. The following simplifying assumptions are made in Model 1:

$$\tau_{d0}^{"} \to 0, X_d^{"} \to X_d^{'}, E_q^{"} \to E_q^{'}$$

to yield the synchronous machine Model 2A. Similarly to Model 1, this is a two-axes generator representation but considering no damper winding in the *d*-axis. The block diagram representation (not shown) is a particular case of the one given in figure 1.

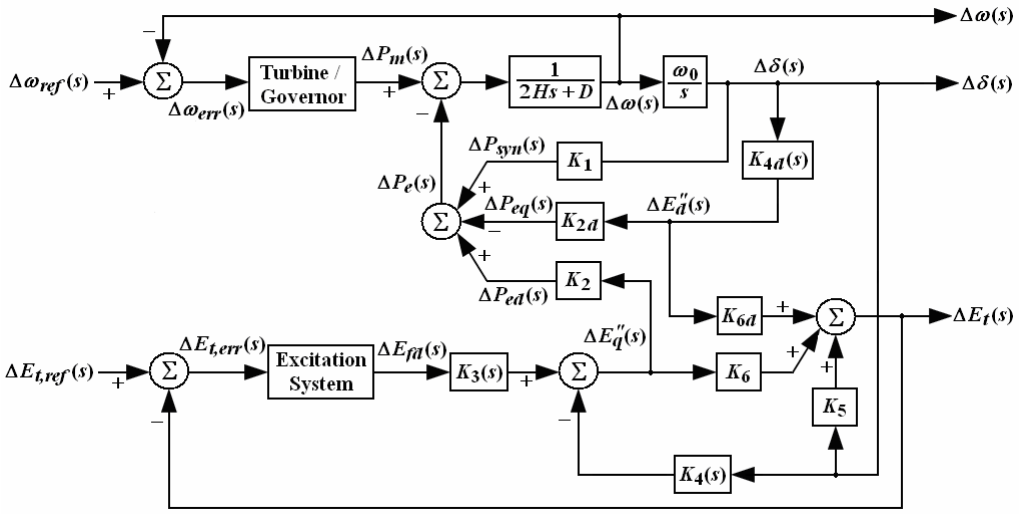

Figure 1. *Block diagram for OMIB system with synchronous generator Model 1*

1.3. Model 2B *(4th order, one-axis)*

With reference to Model 1, the following simplifying assumptions are made to yield Model 2B:

$$\tau''_{q0} \to 0, X''_q \to X_q, E''_d \to 0$$

This 4th order model is essentially a one-axis model with the field winding and one damping winding in the *d*-axis, i.e. no *q*-axis exists. The block diagram representation (not shown) is a particular case of the one given in figure 1.

1.4. Model 3 *(3rd order, one-axis)*

This is the classical model presented by DeMello and Concordia (1969), where the dynamic effects of damping windings are all but neglected. This model may be arrived at by making the following simplifying assumptions in Model 2A

$$\tau''_{q0} \to 0, X''_q \to X_q, E''_d \to 0$$

In this case too, the block diagram representation is a particular case of the one given in figure 1.

1.5. Comparison of models

It is a matter of current interest in ICAD synchronous generator research to determine what should be the correct synchronous generator model to use in order to exact a realistic response of the plant in generator control design tasks, without unduly increasing the overall mathematical complexity. It is reasonable to argue that the higher the model order, i.e. amount of damping winding representation, the closer the model should be to the real machine, but this premise would need to be investigated in detail.

In work related to block diagram representation of OMIB systems, it is already well established by Saidy and Hughes (1994) that higher order models are most desirable by assessing the dynamic characteristics of the system via its frequency response. Following the same approach, in this paper the influence of the simplifications of Models 2A, 2B, and 3 on the dynamic behavior are shown by comparing the Bode plots of their transfer functions $K_3(s)$, $K_4(s)$, and $K_{4d}(s)$ with those of Model 1. The generator operating condition, as well as its parameters, correspond to the lagging power factor operation given by Saidy and Hughes (1994) and can be found in Appendix 1 and 3. The Bode diagrams of the transfer functions given above are shown in figure 2.

The frequency response characteristics can be interpreted as the interaction of one machine variable upon another, such as $\Delta E_q''$ on ΔE_{fd} through $K_3(s)$ (or $\Delta E_q'$ on ΔE_{fd} depending on the model used), $\Delta E_q''$ on $\Delta\delta$ (or $\Delta E_q'$) through $K_4(s)$, and

$\Delta E_d''$ on $\Delta\delta$ through $K_{4d}(s)$. From the Bode plots of the transfer functions $K_3(s)$ and $K_4(s)$ (figure 2), it can be seen that Models 1 and 2B exhibit the same behavior in the frequency domain since their transfer functions are exactly the same; and similarly for Models 2A and 3. The transfer function $K_{4d}(s)$ is only present in Models 1 and 2A and the responses of these models are identical. From these results it can be seen that the response provided by Models 2A and 3, resulting from simplifications made to Model 1, has a higher magnitude and phase lag when compared to the response given by Model 1. Also, a significant difference can be observed in magnitude and a phase lag in $K_4(s)$, especially at higher frequency values.

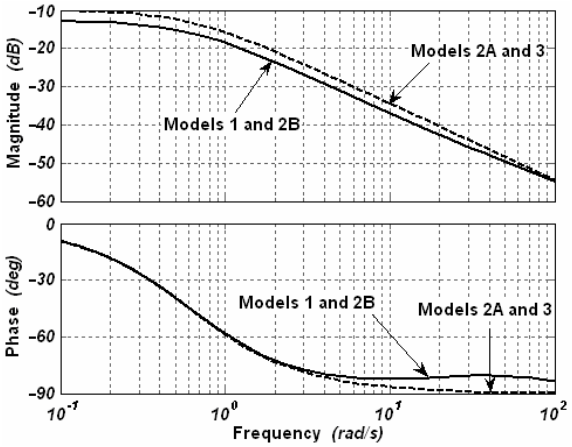

(a)

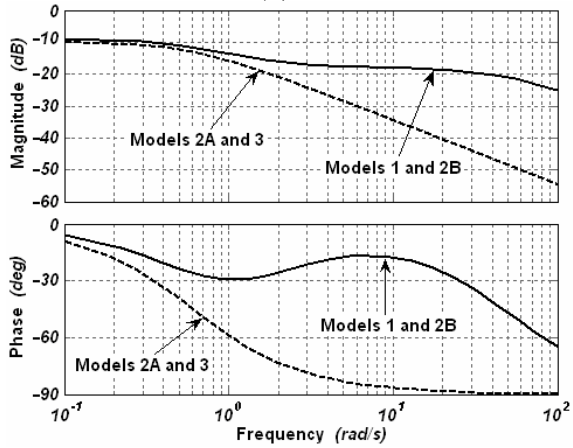

(b)

Figure 2. *Frequency response characteristics for different generator models: (a) $K_3(s)$; (b) $K_4(s)$*

The block diagram representation yields physical insight and understanding of the machine's inner behavior; with the representation enabling a transparent analysis of the interaction between internal machine variables in terms of constants and transfer functions that encapsulate fully all key dynamic parameters of the system. However, caution needs to be exercised since not all interactions between the various variables may be useful for control system design purposes. Equally important, and based on the previous assessment of the bock diagram transfer function models, it is not clear at all which model should be used prior to a control system design, since the frequency response characteristics of Models 1 (two-axes model) and 2B (one-axis) are similar (except for transfer function $K_{4d}(s)$ which does not appear in Model 2B). The same is true for Models 2A (two-axes) and 3 (one-axis). Such ambiguities can be avoided by working with an alternative control-oriented framework termed ICAD, a powerful analysis and design tool which is well suited to the task of carrying out small signal stability assessments of OMIB systems. Throughout the analysis of *Multivariable Structure Functions* (MSF), the dynamical behavior and structure of the system can be described in a global context in which the characteristics of the individual transfer functions do not have a primordial relevance.

2. Transfer Matrix Representation

The transfer matrix representation of the various block diagram models presented in Section 2 can be obtained by suitable manipulation of the relevant equations. Such a representation is not only desirable but essential for analysis of the synchronous generator plant dynamics under the ICAD framework.

The synchronous generator connected to an infinite bus via a tie-line reactance, irrespective of the block diagram model under consideration, has the following generic representation in frequency domain

$$\begin{bmatrix} \Delta\omega(s) \\ \Delta E_t(s) \end{bmatrix} = \begin{bmatrix} g_{11}(s) & g_{12}(s) \\ g_{21}(s) & g_{22}(s) \end{bmatrix} \begin{bmatrix} \Delta P_m(s) \\ \Delta E_{fd}(s) \end{bmatrix} \tag{7}$$

$$\mathbf{y}(s) = \mathbf{G}(s)\mathbf{u}(s) \tag{8}$$

where $\mathbf{G}(s)$ is the transfer matrix of the linearized Models 1, 2A, 2B and 3 of the synchronous generator connected to an infinite bus via a tie-line reactance. The individual elements of $\mathbf{G}(s)$ will vary depending on the selected model.

2.1. Model 1

This model is defined by equations (1)–(6). After some algebraic manipulation, the transfer matrix representation of (7) is obtained, where

$$
\begin{aligned}
g_{11}(s) &= \frac{\left(1+\tau_q^{"}s\right)\left(Es^2+Fs+G\right)s}{den(s)} \\
g_{12}(s) &= -\frac{K_2 A\left(1+\tau_{d0}^{"}s\right)\left(1+\tau_q^{"}s\right)s}{den(s)} \\
g_{21}(s) &= \omega_0\left[\frac{K_5\left(Es^2+Fs+G\right)\left(1+\tau_q^{"}s\right)-K_6\left(B+Cs\right)\left(1+\tau_q^{"}s\right)+K_{6d}C_{4d}\left(Es^2+Fs+G\right)}{den(s)}\right] \\
g_{22}(s) &= \frac{A\left(1+\tau_{d0}^{"}s\right)}{den(s)}\cdot\left[K_6\left(1+\tau_q^{"}s\right)\left(2Hs+D\right)s\right]+ \\
&\quad +\frac{A\left(1+\tau_{d0}^{"}s\right)}{den(s)}\cdot\left(K_6\left[\left(1+\tau_q^{"}s\right)K_1-K_{2d}C_{4d}\right]-K_2\left[\left(1+\tau_q^{"}s\right)K_5+K_{6d}C_{4d}\right]\right)\omega_0
\end{aligned}
\tag{9}
$$

where

$$
\begin{aligned}
den(s) &= \left(2Hs+D\right)\left(Es^2+Fs+G\right)\left(1+\tau_q^{"}s\right)s+K_1\left(Es^2+Fs+G\right)\left(1+\tau_q^{"}s\right)\omega_0+ \\
&\quad -K_2\left(B+Cs\right)\left(1+\tau_q^{"}s\right)\omega_0-K_{2d}C_{4d}\left(Es^2+Fs+G\right)\omega_0
\end{aligned}
$$

and

$$
\begin{aligned}
A &= X_d^{"}+X_{tl} \\
B &= V_{\infty d0}\left(X_d-X_d^{"}\right) \\
C &= V_{\infty d0}\left\{\left(X_d^{'}-X_d^{"}\right)\tau_{d0}^{'}+\left(X_d-X_d^{'}\right)\tau_{d0}^{"}\right\} \\
E &= \tau_{d0}^{'}\tau_{d0}^{"}\left(X_d^{"}+X_{tl}\right) \\
F &= \left[\tau_{d0}^{"}\left\{\left(X_d^{"}+X_{tl}\right)+\left(X_d-X_d^{'}\right)\right\}+\tau_{d0}^{'}\left(X_d^{'}+X_{tl}\right)\right] \\
G &= \left(X_d+X_{tl}\right)
\end{aligned}
$$

2.2. Models 2A, 2B *and* 3

Following a similar line of algebraic manipulations as for Model 1, the corresponding transfer matrix representation is arrived at for the rest of the models. The analysis of the *Multivariable Structure Functions* (MSF) associated to these transfer matrix models enables an effective basis on which to design controllers for the synchronous generator. They also provide for a transparent and

straightforward framework with which to assess the dynamical characteristics of the system. Furthermore, their appropriate interpretation provides a formal explanation as to why some operating conditions are more critical than others. Such insight is not afforded by the block diagram approach.

3. Multivariable Structure Function Analysis

In the framework afforded by ICAD, the dynamical structure of plant (7) is determined by input-output channels resulting from pairing each input to each output by means of diagonal controllers. For instance in the case of the OMIB system, we have

$$\mathbf{K_a}(s)=\begin{bmatrix} k_{11}(s) & 0 \\ 0 & k_{22}(s) \end{bmatrix} \Rightarrow \begin{cases} C_1(s):\Delta P_m(s)\rightarrow \Delta\omega(s) \\ C_2(s):\Delta E_{fd}(s)\rightarrow \Delta E_t(s) \end{cases} \Rightarrow \gamma_a(s)=\frac{g_{12}(s)g_{21}(s)}{g_{11}(s)g_{22}(s)} \tag{10}$$

$$\mathbf{K_b}(s)=\begin{bmatrix} 0 & k_{12}(s) \\ k_{21}(s) & 0 \end{bmatrix} \Rightarrow \begin{cases} C_1(s):\Delta P_m(s)\rightarrow \Delta E_t(s) \\ C_2(s):\Delta E_{fd}(s)\rightarrow \Delta\omega(s) \end{cases} \Rightarrow \gamma_b(s)=\frac{g_{11}(s)g_{22}(s)}{g_{12}(s)g_{21}(s)}=\gamma_a^{-1}(s) \tag{11}$$

A brief summary of ICAD can be found in the Appendix 4. The diagonal controller given in (10), which considers pairings as $\Delta P_m \rightarrow \Delta\omega$ and $\Delta E_{fd} \rightarrow \Delta E_t$, agrees with that used for conventional controllers and this would be the only case here considered, although it is also possible to find a controller associated to (11), where the inputs are swapped.

Coupling between the two channels given in (10) is determined by $\gamma_a(s)$, their associated MSF. A small magnitude of MSF is amenable to a low signal interaction between the governor and exciter loops and vice-versa.

It should be noticed from (9) and (18) that the MSF $\gamma_a(s)$ has an explicit parametrized form which is dependent on the model being used, which is extremely useful in assessing the impact of system parameters changes on system performance, as addressed by Fadlalmoula et al. (1998). For instance, for Model 1 it is given by

$$\gamma_a(s)=\frac{-K_2\left[K_5\left(Es^2+Fs+G\right)\left(1+\tau_q^{*}s\right)-K_6\left(B+Cs\right)\left(1+\tau_q^{*}s\right)+K_{6d}C_{4d}\left(Es^2+Fs+G\right)\right]\omega_0}{\left(Es^2+Fs+G\right)\left\{K_6\left(1+\tau_q^{*}s\right)\left(2Hs+D\right)s+\left(K_6\left[\left(1+\tau_q^{*}s\right)K_1-K_{2d}C_{4d}\right]-K_2\left[\left(1+\tau_q^{*}s\right)K_5+K_{6d}C_{4d}\right]\right)\omega_0\right\}} \tag{12}$$

Two quite different kinds of studies are presented in this section. The first study assesses the behavior of the plant at different operating conditions (power factors) with a fix value of tie-line reactance. The second study assesses the impact of a varying tie-line reactance on system performance and its effect on reactive power requirements. Such operating conditions can be found in the Appendix 3.

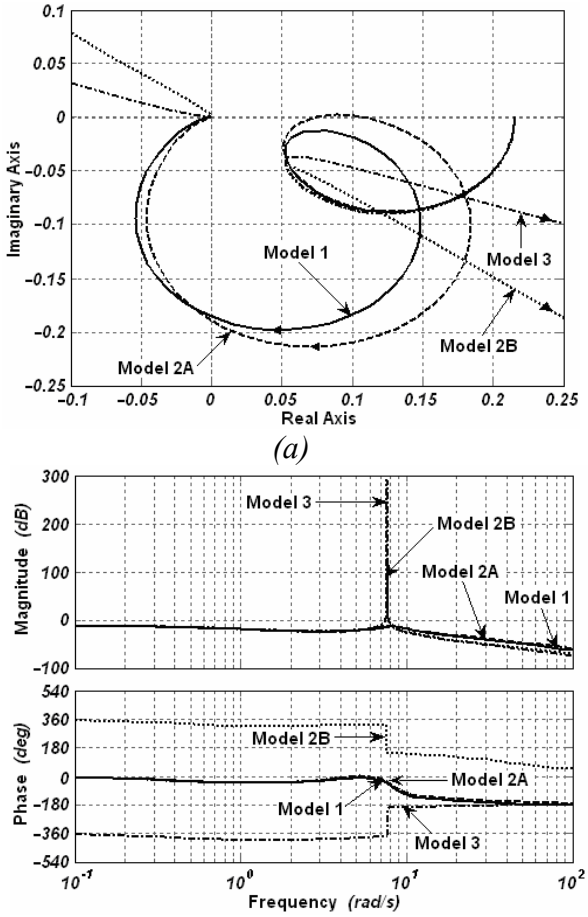

(a)

(b)

Figure 3. *Assessment of $\gamma_a(s)$ (Case I). (a) Nyquist plots; (b) Bode plots*

3.1. Study 1. *Operation under different power factors*

Three cases of power factor values are presented here, which incidentally correspond to previously studied cases using a block diagram approach by Saidy and Hughes (1994). Each case reflects a different operating point of the synchronous generator. Case I corresponds to a lagging power factor, while Case II is for a near-unit power factor, and Case III is for a leading power factor. Parameter information corresponding to such operating conditions is given in Appendix 1. The tie-line reactance is $X_t = 0.2$ *p.u.* in all three cases.

3.1.1. Case I: Lagging Power Factor

Using the operating condition given in the work of Saidy and Hughes (1994) for the case of lagging power factor, the transfer matrices and MSFs of all models are obtained. The Nyquist and Bode diagrams of the MSFs corresponding to our four models are shown in figure 3. As evidenced by the previous set of results, Models 2B and 3 do not yield suitable information for analysis, owing to the absence of a damping winding in the q-axis. Moreover, the awkward switch-back characteristic, typical in these models (which traduces in an unrealistically exaggerated coupling) yields inadequate phase information in the Bode plots. This also explains the differences shown when comparing the Nyquist plots of Models 3 and 2B with those of Models 1 and 2A. Therefore, analysis for the input-output pairing configurations carried out below is restricted to Models 1 and 2A.

The existence and design of stabilizing compensators $k_{11}(s)$ and $k_{22}(s)$ can be determined from the characteristics of $\gamma_a(s)$, revealed by its Nyquist/Bode plots shown in figure 3. An analysis is carried out as in the work of Liceaga-Castro et al. (2005a). It can be concluded that the existence of a stabilizing controller for channels (10) reduces to the existence of controllers $k_{ii}(s)$ which, simultaneously, stabilize both $g_{ii}(s)(1-\gamma_a(s)h_i(s))$ and $g_{ii}(s)$, with $i,j=1,2$, $i\neq j$; that is, a controller that stabilizes both the channels and the diagonal elements of the transfer matrix.

Besides the necessary characteristics that the controllers should have to achieve a closed-loop stable system provided by the analysis of the MSFs, an assessment of the system models should be carried out in order to identify a suitable model for small-signal stability studies. It should be noticed that a zero mechanical damping term D is used as a system parameter in order to assess a more critical condition. Models 1 and 2A offer similar structural characteristics but the latter gives a slightly higher coupling if the pairing associated to conventional controllers is used, as shown in the previous Nyquist/Bode diagrams of the MSFs. Nevertheless, in absence of static damping the behavior of Models 2B and 3 are rather different when compared with Models 1 and 2A. This point is shown all the more clearly when the switch-back characteristic is looked at in the Nyquist/Bode diagrams. Such features may reflect poor performance and poor robustness measures of Models 2B and 3 and not due to a bad controller design in itself.

3.1.2. Case II: Near-Unit Power Factor

As in Case I, Models 2B and 3 have quite different characteristics from those of Models 1 and 2A. Therefore, only Model 1 is analyzed. Figure 4 shows the Nyquist and Bode diagrams of the MSFs for the case of near-unit power factor. Borrowing from the discussion in Case I, in this case too, the existence and design

of stabilizing compensators $k_{11}(s)$ and $k_{22}(s)$ can be determined from the characteristics of $\gamma_a(s)$, revealed by its Nyquist/Bode plots shown in figure 4. The analysis for the case of near-unit power factor does not differ significantly from that of lagging power factor; hence, no further discussion is warranted.

3.1.3. Case III: Leading Power Factor

The Nyquist and Bode plots of the MSFs associated to Model 1 are shown in figure 4 for the case of leading power factor operation. The existence of controllers is determined by the characteristics of the MSFs, reflected by their Bode and Nyquist plots. The analysis carried out for Case I is also applied to the case of lagging power factor.

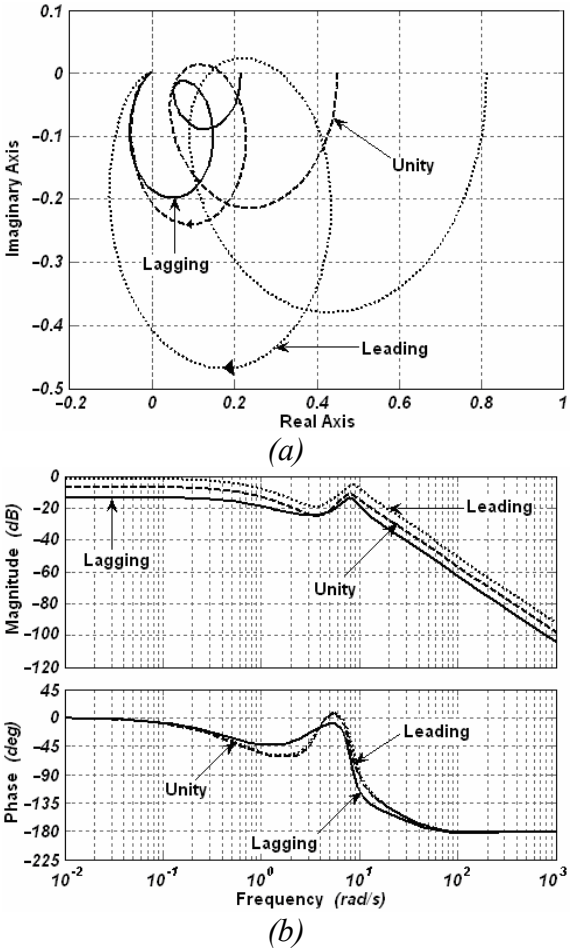

(a)

(b)

Figure 4. *Assessment $\gamma_a(s)$ of Model 1 at three different power factor conditions: (a) Nyquist plots; (b) Bode plots.*

As a corollary of the previous analysis, it may be stated, in quite broad terms, that independently of the operating points at which the synchronous generator finds itself, the existence of a stabilizing controller for channels (10) (considering parings: $\Delta P_m \rightarrow \Delta\omega$ and $\Delta E_{fd} \rightarrow \Delta E_t$) reduces to the existence of controllers $k_{ii}(s)$ which stabilize simultaneously $g_{ii}(s)(1-\gamma_a(s)h_i(s))$ and $g_{ii}(s)$, with i,j=1,2, $i \neq j$. In other words, if a multivariable controller is obtained in which the characteristics of the MSFs are addressed correctly, such fixed controller should guarantee stability and robustness for all operating conditions.

Figure 4 shows the Nyquist and Bode plots of γ_a(s) of Model 1 for all operating conditions assessed in Study 1. In all conditions, the phase margin is infinite. Notice that if conventional controllers are used the most critical operating condition is when the generator works at a leading power factor because $\gamma_a(0)$ approaches the point (1,0) (i.e. the gain margin is small). As seen, the coupling between channels in this case starts to be considerable. Also, stability robustness decreases as the Nyquist plot moves toward (1,0). Similarly, an increase in active power is associated with a decrease in stability robustness. Such characteristics are consistent with what has been observed in practice. Also, the Nyquist plot always starts to the left of the point (1,0) –an important fact, since the structural characteristics are preserved for all the cases here presented. In other words, it can be stated that the system is minimum phase and stable for all operating conditions.

Notice that the polar plots of $\gamma_a(s)$ (figure 3, lagging power factor condition) clearly show that models 2B and 3 contain no damping at the natural oscillation frequency and, as a result, a high switch-back characteristic is present. By addition of the *q*-axis damper in the models, as in Models 1 and 2A, system damping is introduced over the frequency range of concern. It can be concluded that models 2B and 3, including only winding representation in the *d*-axis, do not yield sufficient system damping representation and are not recommended for analysis and control system design. Models 1 and 2A offer similar structural characteristics to one another; however, Model 1 exhibits a higher level of reliability and accuracy. Whenever computational burden is not an issue, Model 1 should be used.

3.2. *Study* 2. *Operation with different tie-line reactances*

An assessment of synchronous generator performance is carried out under different values of tie-line reactance under lagging power factor conditions. Such study is carried out as by Saidy and Hughes (1994), where values of tie-line reactance considered are X_{tl} = 0.2, 0.4, 0.6, 0.8 *p.u.* Model 1 is the only one considered in this study. The Nyquist and Bode plots of the associated MSFs for the four tie-line reactances are shown in figure 5.

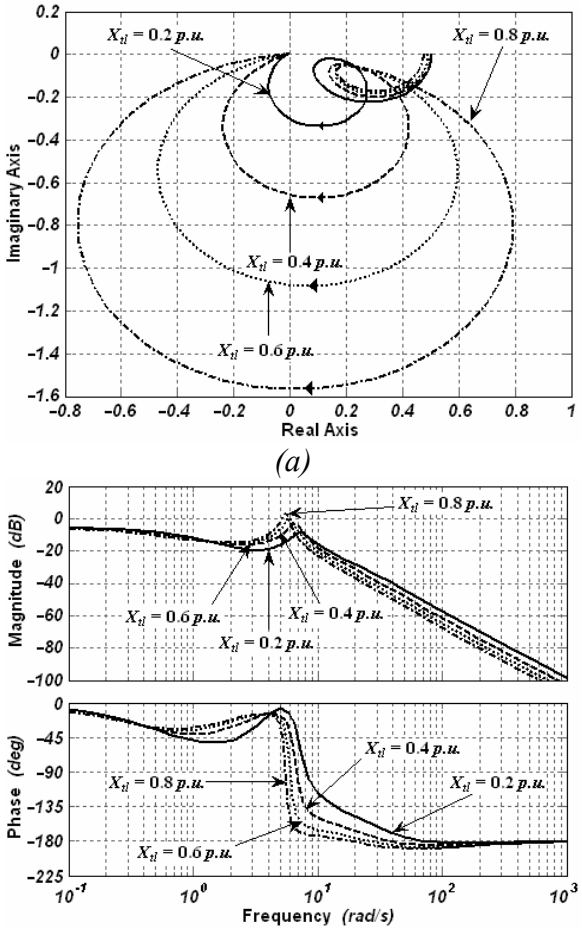

Figure 5. *Assessment of $\gamma_a(s)$ at different tie-line reactances: (a) Nyquist plots; (b) Bode plots.*

As previously discussed, the existence of stabilizing controllers is determined by the characteristics of the MSF. The analysis in all cases is carried out in a similar manner as in Case I of Study 1, since the structural characteristics under varying tie-line reactance are preserved. In fact, γ_a(s) offers a gain margin of around 5.9 *dB* for all values of the tie-line reactance and the Nyquist plot always starts to the left of (1,0). It should be noticed that the coupling between channels increases if the value of the tie-line reactance grows. For the cases when X_{tl} = 0.6, 0.8 *p.u.* coupling over 0 *dB* is present for a range of frequencies, as evidenced by the Bode diagram. This is consistent with the fact that for long-distance transmission, with no VARs compensation plant, system operation becomes impaired because of the long electrical distances involved. One other key

observation elucidated from the previous analysis is that the larger the amount of reactive power flow in the tie-line reactance (while keeping active power constant), the higher the coupling between channels –and thus becoming difficult to control the plant.

It is argued by Saidy and Hughes (1994) that the block diagram representation provides a useful basis for the analysis of the generator dynamic performance. It should be noticed, however, that the frequency response plots of the individual transfer functions offer little information about the structure and characteristics that the controllers should possess in order to have a stable and robust control system. In contrast, an appropriate analysis (at low and high frequencies) of the MSF gives an effective and complete framework for designing multivariable control systems. In fact, the MSF analysis dictates what characteristics the controllers should have in order to assure closed-loop stability and robustness. It also provides a measurable quantification of coupling between the input-output channels, information which is available in the frequency domain. Moreover, the MSFs show in a clear and simple manner why some operating conditions are more critical than others.

3.3. A note on the models

As it was concluded previously, following a detailed MSF study, Models 1 and 2A are more suitable for control system design. This is further qualified by assessing the actual performance of all models. It should be noticed that a zero mechanical damping term D is used as a system parameter in order to assess a more critical condition. It may be argued that there is always some damping present in a physical machine and that the differences between Models 3 and 2B and Models 1 and 2A may be exaggerated if such an effect is not explicitly included. To prove this point or otherwise, and in order to examine thoroughly the effect of the static damping, figure 6(a) presents a comparison between the MSF of Model 1 considering $D = 0$ and with $D = 2.5$. The Bode plot reveals no major differences between them. The effect of not including the static damping in this model, which already accounts for dynamic damping provided by the damping windings, is practically negligible.

Moreover, figure 6(b) shows the MSFs of the four models when a static damping of $D = 2.5$ is considered. Models 1 and 2A agree on well throughout the frequency range. In contrast, the frequency response characteristics obtained with Models 2B and 3 (one-axis models) only coincide with those of the two-axes models at low frequencies, up to ≈6 *rad/s*. It should also be noticed that the inclusion of damping, $D = 2.5$, in models 2B and 3 do not dent the awkward switch-back characteristic.

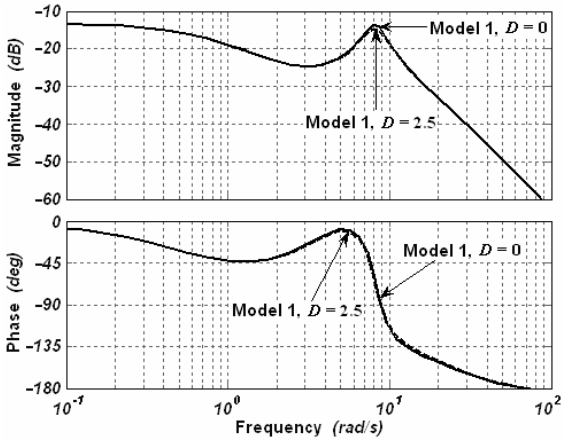

(a)

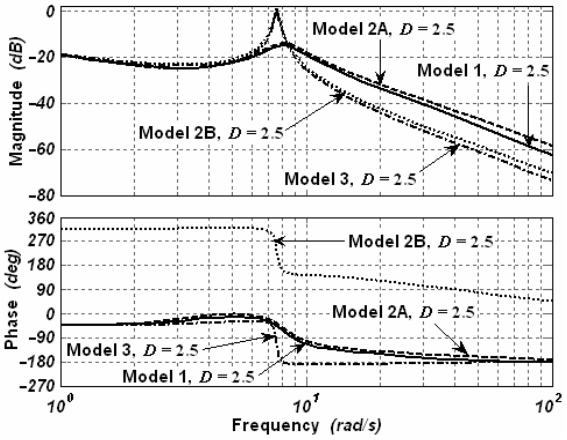

(b)

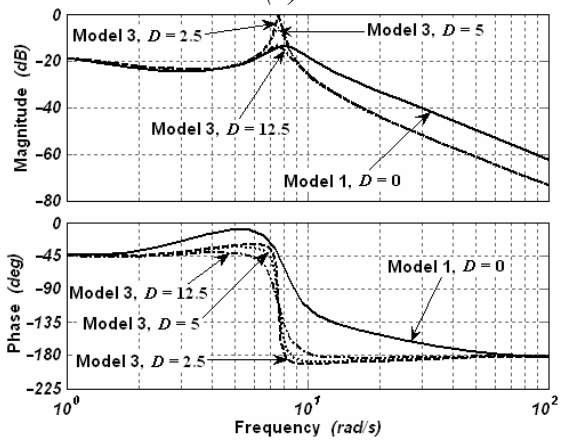

(c)

Figure 6. *Assessment of the static damping term D. Bode plots of $\gamma_a(s)$: (a) Model* 1 *for D* = 0 *and* 2.5*; (b) all Models with D* = 2.5*; (c) Model* 3 *at different values of D vs Model* 1 *with D* = 0.

Figure 6(c) shows the MSF using Model 1 with zero mechanical damping and that of Model 3 including three damping terms D greater than zero, for a lagging power factor operation. As shown, differences between the two models are very significant even for the case when a large value of D is used, e.g. 12.5. Furthermore, differences between the magnitudes and phases in the Bode plots are also noticeable between the two models. In fact, for values of D in the range 2–5, the MSFs show the presence of the awkward switch-back characteristic when Model 3 is applied. As the MSF provides a measure of coupling, one may think that a higher coupling exists between the channels if Model 3 is used, which happens to not be the case. Use of Model 3, with or without artificial damping D, will lead to a poor performance due to an inaccurate model.

It may be said that Models 2B and 3, whose winding representation is confined to the *d*-axis, do not yield enough system damping. Therefore, the use of such models for small-signal stability studies may lead to inaccurate analysis due to a poor performance arising from inherent short-comings in such models and not due to a bad control system design at all. Whenever it is required that a model exhibits a realistic dynamic behavior throughout all the frequency range, including the rotor mechanical oscillation frequency (≈7.5 *rad/s*) and higher frequencies, one-axis models should be avoided. Although Model 2A can be used for small-signal stability studies, Model 1 provides a higher level of reliability.

4. Conclusion

ICAD provides an alternative, very insightful framework with which to carry out small-signal stability assessments of OMIB systems. It shows analytical advantages over the physically-oriented block diagram method. Also, a suitable analysis of the MSF, at low and high frequencies, is amenable to a complete multivariable control system design. Moreover, its correct interpretation provides simple and straightforward designs. In addition, a quantification of the coupling between input and output transmission channels becomes readily available and it provides a formal explanation as to why some operating conditions are more critical than others.

It is concluded in the paper that two-axes synchronous generator models should be preferred over one-axis models, since the latter have been found to be system damping deficient –a conclusion reached after having performed comprehensive studies using both ICAD and the physically-oriented block-diagram approach. As shown, one-axis models may lead to inaccurate analysis and a poor control system performance due to the inferior quality of the model used and not to a bad controller in itself. Among the two-axes models, Model 1 should be preferred over Model 2A, owing to its superior reliability and performance at high frequencies.

Simulation results obtained are in agreement with system behavior observed in practice. It was shown that the most critical operating condition occurs at leading power factor. Coupling between channels is higher during leading power factor operation than under lagging or near-unit power factor operation, resulting in a considerable loss of robustness. It was also noticed that channel coupling increases with electrical distance, decreasing stability robustness. The study of the control system design and stability and structural robustness assessment is addressed in Part 2 of this paper. Work is under way to generalize a multi-machine model and to include FACTS devices.

Appendix 1. System parameters

Base power: 100 *MVA*.
Synchronous generator: 6 *p.u.*

Table I. *Synchronous Machine Parameters*

Variable	Value
X_d	1.445 *p.u.*
X'_d	0.316 *p.u.*
X''_d	0.179 *p.u.*
τ'_{d0}	5.26 *s*
τ''_{d0}	0.028 *s*
X_q	0.959 *p.u.*
X''_q	0.162 *p.u.*
τ''_{q0}	0.159 *s*
R_a	0
D	0
H	4.27
X_t	0.2 *p.u.*
f_0	50 *Hz*

Appendix 2. System coefficients and transfer functions (Model 1)

$$K_1 = \frac{V_{\infty d0}^2}{X_d^{"} + X_{tl}} + \frac{V_{\infty q0}^2}{X_q^{"} + X_{tl}} - I_{q0}V_{\infty d0} + I_{d0}V_{\infty q0}$$

$$K_2 = \frac{V_{\infty d0}}{X_d^{"} + X_{tl}} \qquad K_{2d} = \frac{V_{\infty q0}}{X_q^{"} + X_{tl}}$$

$$K_3(s) = \frac{1}{D(s)} \cdot \left(1 + \tau_{d0}^{"} s\right)\left(X_d^{"} + X_{tl}\right)$$

$$K_4(s) = \frac{V_{\infty d0}}{D(s)}\left[\left(X_d - X_d^{"}\right) + \left\{\left(X_d^{'} - X_d^{"}\right)\tau_{d0}^{'} + \left(X_d - X_d^{'}\right)\tau_{d0}^{"}\right\} s\right]$$

$$D(s) = \tau_{d0}^{'}\tau_{d0}^{"} s^2\left(X_d^{"} + X_{tl}\right) + \left[\tau_{d0}^{"}\left\{\left(X_d^{"} + X_{tl}\right) + \left(X_d - X_d^{'}\right)\right\} + \tau_{d0}^{'}\left(X_d^{'} + X_{tl}\right)\right] s + \left(X_d + X_{tl}\right)$$

$$K_{4d}(s) = \left(\frac{C_{4d}}{1 + \tau_q^{"} s}\right) \qquad C_{4d} = \left(\frac{X_q - X_q^{"}}{X_q + X_{tl}}\right) \cdot V_{\infty q0}$$

$$K_5 = \left[\frac{E_{td0}}{E_{t0}} \cdot \frac{X_q^{"} V_{\infty q0}}{X_q^{"} + X_{tl}} - \frac{E_{tq0}}{E_{t0}} \cdot \frac{X_d^{"} V_{\infty d0}}{X_d^{"} + X_{tl}}\right]$$

$$K_6 = \left[\frac{E_{tq0}}{E_{t0}} \cdot \frac{X_{tl}}{X_d^{"} + X_{tl}}\right] \qquad K_{6d} = \left[\frac{E_{td0}}{E_{t0}} \cdot \frac{X_{tl}}{X_q^{"} + X_{tl}}\right] \qquad \tau_q^{"} = \left(\frac{X_q^{"} + X_{tl}}{X_q + X_{tl}}\right)\tau_{q0}^{"}$$

Appendix 3. System operating conditions

Table II. *System operating condition for Study* 1

	Value		
Variable	**Case I**	**Case II**	**Case III**
P_g	0.736 *p.u.*	0.832 *p.u.*	0.912 *p.u.*
Q_g	0.7518 *p.u.*	0.1277 *p.u.*	–0.3921 *p.u.*
δ_0	29.85°	41.72°	58.85°
$\lvert V_\infty \rvert$	0.92 *p.u.*	1.04 *p.u.*	1.14 *p.u.*
$\angle V_\infty$	60.15°	48.28°	31.15°
$\lvert E_t \rvert$	1.0522 *p.u.*	1.0522 *p.u.*	1.0522 *p.u.*
$\angle E_t$	68.89°	57.03°	39.91°
E_{fd0}	2.309 *p.u.*	1.652 *p.u.*	1.29 *p.u.*
$V_{\infty q0}$	0.79794 *p.u.*	0.77626 *p.u.*	0.5897 *p.u.*
$V_{\infty d0}$	0.45791 *p.u.*	0.69211 *p.u.*	0.97563 *p.u.*
E_{t0}	1.0522 *p.u.*	1.0522 *p.u.*	1.0522 *p.u.*
E_{tq0}	0.98159 *p.u.*	0.88275 *p.u.*	0.67507 *p.u.*
E_{td0}	0.37896 *p.u.*	0.57261 *p.u.*	0.80709 *p.u.*
I_0	0.999 *p.u.*	0.79998 *p.u.*	0.94347 *p.u.*
I_{q0}	0.39521 *p.u*	0.59734 *p.u*	0.84194 *p.u*
I_{d0}	0.91848 *p.u.*	0.53213 *p.u.*	0.42576 *p.u.*

Table III. *System operating condition for Study* 2

Variable	Value			
	Case A X_{tl} = 0.2 *p.u.*	**Case B** X_{tl} = 0.4 *p.u.*	**Case C** X_{tl} = 0.6 *p.u.*	**Case D** X_{tl} = 0.8 *p.u.*
$_g$	0.736 *p.u.*	0.736 *p.u.*	0.736 *p.u.*	0.736 *p.u.*
P_g	0.128 *p.u.*	0.256 *p.u.*	0.384 *p.u.*	0.512 *p.u.*
Q	45.22°	49.76°	53.58°	56.82°
$\delta_{0\infty}\|$	0.92 *p.u.*	0.92 *p.u.*	0.92 *p.u.*	0.92 *p.u.*
$\|V_{V_\infty}$	44.78°	40.24°	36.42°	33.18°
$\angle$ |	0.9338 *p.u.*	0.9741 *p.u.*	1.0377 *p.u.*	1.1207 *p.u.*
$\|E_{E_t}$	54.64°	59.42°	63.97°	68°
$\angle_0$	1.5822 *p.u.*	1.721 *p.u.*	1.8627 *p.u.*	2.0067 *p.u.*
$E_{fd_{q0}}$	0.64804 *p.u.*	0.59431 *p.u.*	0.5462 *p.u.*	0.50349 *p.u.*
$V_{\infty_{d0}}$	0.65303 *p.u.*	0.70228 *p.u.*	0.74031 *p.u.*	0.77 *p.u.*
V_{∞_0}	0.9338 *p.u.*	0.9741 *p.u.*	1.0377 *p.u.*	1.1207 *p.u.*
E_{t_0}	0.76154 *p.u.*	0.83862 *p.u.*	0.93244 *p.u.*	1.0391 *p.u.*
E_{tq_0}	0.5404 *p.u.*	0.49556 *p.u.*	0.45539 *p.u.*	0.41982 *p.u.*
E_{td}	0.80001 *p.u.*	0.79997 *p.u.*	0.79999 *p.u.*	0.80001 *p.u.*
I_{0_0}	0.56346 *p.u.*	0.51678 *p.u.*	0.47492 *p.u.*	0.43777 *p.u.*
I_{q_0}	0.56792 *p.u.*	0.61064 *p.u.*	0.64377 *p.u.*	0.66961 *p.u.*
I_d				

Appendix 4. A brief summary of Individual Channel Analysis and Design

In a typical control design task the performance is specified in terms of an output response to a given input. Nevertheless, the multivariable control design problem is inherently interactive in nature with an interplay between plant attributes, customer specification, and the design process itself (O'Reilly and Leithead, 1991). For clarity of both performance specification and design, it remains desirable to consider the inputs and outputs in pairs. Input r_i is paired with output y_i in accordance with specifications. An individual pairing is called a channel. Then, channel C_i is the pairing between r_i and y_i, as defined by Leithead and O'Reilly (1991). When the plant cross–coupling is weak, the design task reduces to a set of SISO design tasks and a scalar controller can be designed separately for each channel. In such context, the most appropriate methodology is to apply classical Nyquist/Bode analysis and design to each channel.

Individual Channel Analysis and Design (ICAD), introduced by O'Reilly and Leithead (1991), is a framework in which Bode/Nyquist techniques can be applied directly to the channels not only when cross-coupling is weak but in all circumstances including when cross-coupling is strong. The multivariable system is represented as an equivalent set of SISO systems. Each SISO system is the open-loop channel transmittance between input r_i and output y_i, with the feedback loop between output y_i and input r_i open but all other feedback loops closed, for a particular choice of i. What is particular to ICAD is that the SISO channel transmittances are reformulated to make explicit the role of the plant structure. Scalar Multivariable Structure Functions (MSFs) to which the individual channel transmittances are simply related encapsulate the significant aspects of the plant structure. The multivariable nature of the original plant is maintained in the equivalent SISO systems through the MSFs with no loss of information, as shown by O'Reilly and Leithead (1991) and Leithead and O'Reilly (1991).

ICAD seeks to provide the potential user with a design framework for multivariable feedback control systems that is transparent, flexible and capable of validation against observed plant data, building confidence in the arrived-at design, and being well-suited to the specific engineering context, as discussed by O'Reilly and Leithead (1991).

The ICAD set up for a 2–input 2–output plant is shown next for completeness, as in the work of Leithead and O'Reilly (1991), since the OMIB system corresponds to a 2x2 plant. Let

$$\mathbf{Y}(s) = \mathbf{G}(s)\mathbf{u}(s) \tag{13}$$

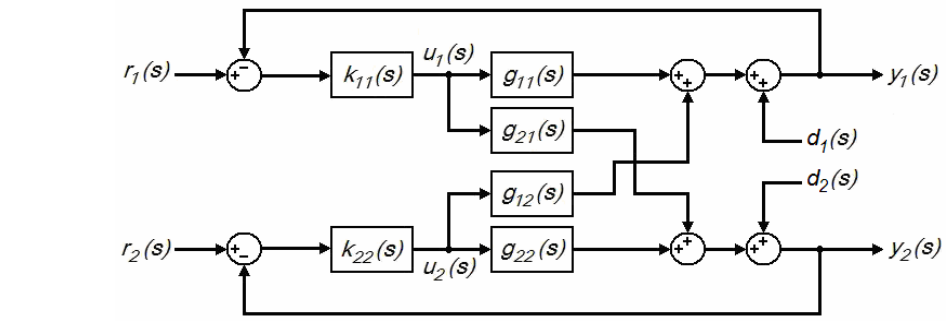

(a)

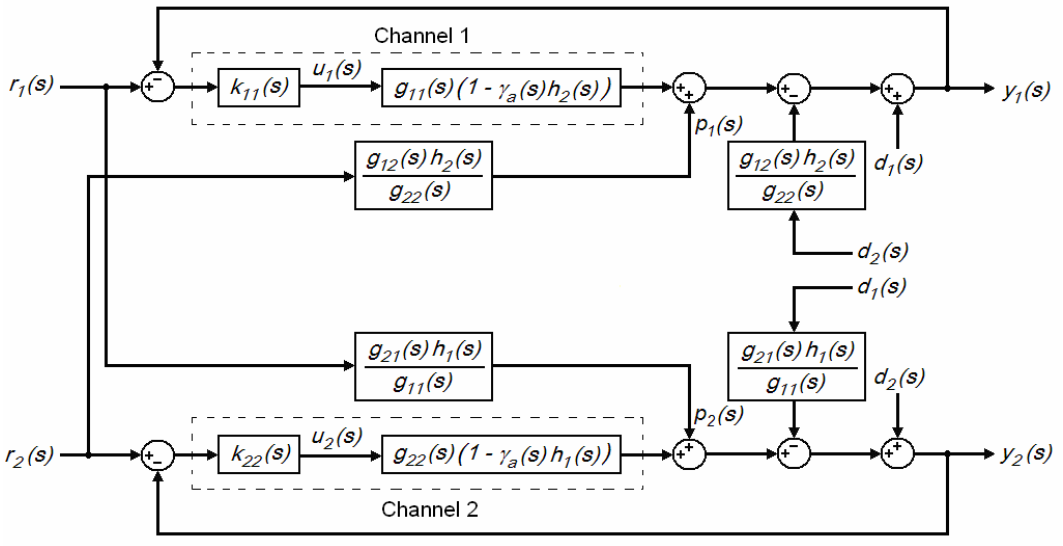

(b)

Figure 7. *(a) The 2x2 multivariable system with diagonal controller; (b) Channel representation*

be a 2*x*2 plant represented by

$$\begin{bmatrix} y_1(s) \\ y_2(s) \end{bmatrix} = \begin{bmatrix} g_{11}(s) & g_{12}(s) \\ g_{21}(s) & g_{22}(s) \end{bmatrix} \begin{bmatrix} u_1(s) \\ u_2(s) \end{bmatrix} \tag{14}$$

where $g_{ij}(s)$ represents scalar transfer functions, $y_i(s)$ the outputs, and $u_i(s)$ the inputs of the system, with $i,j = 1,2$. If a diagonal controller is given by

$$\mathbf{u}(s) = \mathbf{K}(s)\mathbf{e}(s) \tag{15}$$

$$\begin{bmatrix} u_1(s) \\ u_2(s) \end{bmatrix} = \begin{bmatrix} k_{11}(s) & 0 \\ 0 & k_{22}(s) \end{bmatrix} \begin{bmatrix} e_1(s) \\ e_2(s) \end{bmatrix} \tag{16}$$

with $e_i(s) = r_i(s) - y_i(s)$, where $r_i(s)$ represents the plant references, then the open loop input-output channels are clearly defined from figure 7 as

$$C_i(s) = k_{ii}(s)\, g_{ii}(s)\left(1 - \gamma_a(s) h_j(s)\right) \tag{17}$$

where $i \neq j$ and $i,j = 1,2$. The complex valued function

$$\gamma_a(s) = \frac{g_{12}(s) g_{21}(s)}{g_{11}(s) g_{22}(s)} \tag{18}$$

is referred to as the Multivariable Structure Function (MSF). The functions $h_i(s)$ are:

$$h_i(s) = \frac{k_{ii}(s) g_{ii}(s)}{1 + k_{ii}(s) g_{ii}(s)} \tag{19}$$

The interaction or cross coupling between the channels can be evaluated through a transfer function. For instance, the influence of channel–j on channel–i is (figure 7(b)):

$$p_i(s) = \frac{g_{ij}(s)}{g_{jj}(s)} h_j(s) r_j(s) \tag{20}$$

The block diagram of the feedback system with the diagonal controller is shown in figure 7(a) and the equivalent scalar channels are shown in figure 7(b). Considering the OMIB system, it should be noted that the controller $k_{11}(s)$ stands for the turbine/governor system and $k_{22}(s)$ for the excitation system, respectively.

It is clear that the correct interpretation of the MSF (18) is of great importance, as discussed by Liceaga-Castro et al. (2005a), because

- It determines the dynamical characteristics of each input-output configuration;
- It has an interpretation in the frequency domain;
- Its magnitude quantifies the coupling between the channels (in the frequency domain);
- It is related to the plant transmission zeros;
- $\gamma_a(s) = 1$ determines the non-minimum phase condition;
- Its closeness to (1,0) in the Nyquist plot indicates to what extent the plant is sensitive to uncertainty in terms of gain and phase margins. This fact plays a key role in the design of *robust controllers*.

It should be emphasized that in the individual channel representation of the multivariable system there is no loss of information. The multivariable character and cross coupling of the plant are contained in the MSF and the cross coupling terms. That is, (13)–(20) are equivalent to the closed-loop matrix function

$$\mathbf{G}_{\mathbf{cl}}(s) = \left(\mathbf{I} + \mathbf{G}(s)\mathbf{K}(s)\right)^{-1} \mathbf{G}(s)\mathbf{K}(s) \tag{21}$$

It can be proven that in order to stabilize (21) it is just necessary to stabilize the channels given by (17). In general, stabilization of the diagonal elements of $\mathbf{G}(s)$ is not required. The open loop system dynamical structure with a diagonal controller is summarized in Table IV, as given by Leithead and O'Reilly (1991).

Table IV. *Dynamical structure of open loop channels*

Channel	Zeros	Poles
$C_1(s)$	Zeros of $(1-\gamma_a(s)h_2(s))$	Poles of $g_{11}(s)$, $g_{12}(s)$, $g_{21}(s)$, $h_2(s)$
$C_2(s)$	Zeros of $(1-\gamma_a(s)h_1(s))$	Poles of $g_{22}(s)$, $g_{12}(s)$, $g_{21}(s)$, $h_1(s)$

Notice that the coupling can be expressed in decibels directly from the channels (17) by means of functions $\gamma_a(s)h_j(s)$. On the other hand, it is possible to determine the dynamical structure of the system using Table IV and analyzing the Nyquist plot of $(1-\gamma_a(s)h_j(s))$.

The controller performance characteristics are determined by the MSF. Moreover, the robustness of the channels can be established in terms of gain and phase margins as the Nyquist paths of the functions $\gamma_a(s)h_i(s)$ do not pass near (1,0). Thus the design of $k_{ii}(s)$, which should provide adequate gain and phase margins for $k_{ii}(s)g_{ii}(s)$, can be obtained through an iterative process.

References

Aree, P. and Acha, E. "Block diagram model for fundamental studies of a synchronous generator – static VAR compensator system." *IEE Proceedings on Generation, Transmission and Distribution,* **146(5)**, pp. 507–514, 1999.

DeMello, F.P. and Concordia, C. "Concepts of synchronous machine stability as affected by excitation control." *IEEE Transactions on Power Apparatus and Systems,* **88(4)**, pp. 316–329, 1969.

Dudegon, G.J.W.; Leithead, W.E.; O'Reilly, J.; and McDonald, J.R. "Prospects for the Decentralised Control of Small-Scale Power Networks with Embedded Generation." *Proceedings of the IEEE Power Engineering Society Summer Meeting*, **2(2)**, pp. 1399–1404, 2000.

Edwards, F.V.; Dudgeon, G.J.W.; McDonald, J.R.; and Leithead, W.E. "Dynamics of Distribution Networks with Distributed Generation." *Proceedings of the IEEE Power Engineering Society Summer Meeting 2000*, **2(2),** pp. 1032–1037, 2000.

Fadlalmoula, Z.; Robertson, S.S.; O'Reilly, J.; and Leithead, W.E. "Individual channel analysis of the turbogenerator with a power system stabilizer." *International Journal of Control,* **69(2)**, pp. 175–202, 1998.

Hammons, T.J. and Winning, D.J. "Comparisons of synchronous – machine models in the study of the transient behavior of electrical power systems." *IEE Proceedings*, **118(10)**, pp. 1442–1458, 1971.

Heffron, W.G. and Phillips, R.A. "Effects of modern Amplidyne voltage regulator in under excited operation of large turbine generators." *IEEE Transactions in Power Apparatus and Systems*, **71**, pp. 692–697, 1952.

Kundur, P.; Rogers, G.J.; Wong, D.Y.; Wang, L.; and Lauby, M.G. "A comprehensive computer program package for small signal stability analysis of power systems." *IEEE Transactions in Power Systems*, **5(4)**, pp. 1076–1083, 1990.

Leithead, W.E. and O'Reilly, J. "Performance issues in the individual channel 2-input 2-output systems. Part I: Structural issues." *International Journal of Control*, **54(1)**, pp. 47–82, 1991.

Licéaga-Castro, E.; Licéaga-Castro, J.; and Ugalde-Loo, C.E. "Beyond the Existence of Diagonal Controllers: from the Relative Gain Array to the Multivariable Structure Function." *Proceedings of the Joint 44th IEEE Conference on Decision and Control and the European Control Conference 2005*, pp. 7150–7156, 2005.

Licéaga-Castro, E.; Ugalde-Loo, C.E.; Licéaga-Castro, J.; and Ponce, P. "An Efficient Controller for SV-PWM VSI Based on the Multivariable Structure Function." *Proceedings of the Joint 44th IEEE Conference on Decision and Control and the European Control Conference 2005*, pp. 4754–4759, 2005.

Licéaga-Castro, E.; Ugalde-Loo, C.E.; and Licéaga-Castro, J. "Induction Motor Control by Individual Channel Analysis and Design." *Proceedings of the International Conference Control 2006*, Glasgow, Scotland, UK, 2006.

O'Reilly, J. and Leithead, W.E. "Multivariable control by 'individual channel design'." *International Journal of Control,* **54(1),** pp. 1–46, 1991.

Rogers, G. *Power System Oscillations*. Kluwer Academic Publishers, Massachusetts, USA, 2000.

Saidy, M. and Hughes, F.M. "Block diagram transfer function model of a generator including damper windings." *IEE Proceedings on Generation, Transmission and Distribution,* **141(6)**, pp. 599–608, 1994.

Ugalde-Loo, C.E.; Olguin-Salinas, D.; Licéaga-Castro, E.; and Licéaga-Castro, J. "Individual Channel Design for Synchronous Generators." *International Journal of Emerging Electric Power Systems,* **4(2)**, article 4, 2005. (http://www.bepress.com/ijeeps/vol4/iss2/art4).

Ugalde-Loo, C.E.; Vanfretti, L.; Licéaga-Castro, E.; Acha, E. "Synchronous Generator Control: from the traditional perspective to the ICAD framework." *Proceedings of the International Conference Control 2006*, Glasgow, Scotland, UK, 2006.